AIAA JOURNAL
Vol. 40, No. 4, April 2002

Mixing Enhancement of Compressible Jets by Using Unsteady Microjets as Actuators

Mohammed K. Ibrahim,* Ryoji Kunimura,† and Yoshiaki Nakamura‡
Nagoya University, Nagoya 464-8603, Japan

Lateral steady/unsteady injection of an array of microjets, which are placed along the circumference of the nozzle exit of a primary jet at equal intervals of azimuthal angle, was studied experimentally to clarify the characteristics of mixing and noise of compressible primary jets. Two modes of the microjets were investigated: axisymmetric and antisymmetric injections. Fully expanded and underexpanded primary jets issued from a convergent nozzle are considered in the present study. The unsteady microjets were injected at a Strouhal number *Sr* of 0.16, based on the nozzle exit diameter and the velocity at the nozzle exit, for two cases of total mass injection: 4 and 6% of primary jet mass flow rate. Results of the mean flowfield showed that the antisymmetric injection has a higher spreading rate than the steady and unsteady axisymmetric injections in terms of centerline velocity decay. Those results were confirmed from linear stability analysis, which showed that antisymmetric modes for natural disturbances are more unstable in the downstream region than the corresponding axisymmetric modes. Moreover, reduction in the radiated noise was observed in steady axisymmetric injection. Thus, these results suggest that unsteady microjets have the potential for future use as a device for shear flow control.

Nomenclature

D = nozzle exit diameter
f = injection frequency of microjets
i = $\sqrt{-1}$
M = Mach number
M_j = fully expanded jet Mach number; Mach number the jet will have when isentropically expanded to the ambient pressure
n = azimuthal wave number of disturbance; jet instability mode
p = pressure
Pr = Prandtl number
P_t = jet total pressure; chamber pressure
P_μ = total pressure of micro jet; microchamber pressure
Re = Reynolds number
$R_{0.5}$ = jet radius defined as the length from the axis to the location where the velocity becomes half the centerline velocity, that is $U(R_{0.5}) = U_o/2$
Sr = Strouhal number, fD/U
T = temperature
U = velocity
α = $\alpha_r + i\alpha_i$
α_i = axial spatial growth rate of disturbance
α_r = axial wave number of disturbance
γ = specific heat ratio
θ = momentum thickness
ρ = density
τ = period of injection cycle
φ_j = injected mass fraction defined as the ratio of injected mass to the primary jet mass flow rate
ψ = sound emission angle from the jet axis
Ω = driving motor's rotational speed, rpm
ω = radian frequency of disturbance

Subscripts

0 = primary jet centerline condition
∞ = ambient condition; in the far field

I. Introduction

THERE are many technological applications regarding jet mixing enhancement. For example, enhanced jet mixing can reduce temperature on in-plume aerodynamic surfaces, which provides greater flexibility in the choice of materials for their construction.[1] Similarly, the mixing efficiency of fuel jets in combustors is an important factor in their overall performance, where reductions in their size and weight will be possible if the mixing can be improved.

Jets and mixing layers are characterized by their mean-velocity profiles with an inflection point that causes inviscid instabilities. The primary mechanism of these instabilities is the so-called vortical induction, where viscosity plays only a role of damping. Major goals for such flow control are mixing enhancement and noise suppression. In general, two kinds of control, active and passive, can be considered. Examples of the passive control are tabs that are located at the nozzle exit,[2] crown-shaped nozzle,[3] and various other tailorings of the nozzle exit.[4] Passive control is attractive because in many cases it entails only simple design modifications. On the other hand, active control, where nozzle conditions are continuously updated through a feedback loop, has greater flexibility, and therefore greater potentials to change the jet flow.

Previous studies on shear layer dynamics and jet mixing control have often employed acoustic drivers because such drivers can produce almost axisymmetric and/or azimuthal modes at any desired frequency and amplitude. These acoustic drivers are valuable in providing insight into the physics of shear layer flow. However, they are not suitable for controlling flows of practical interest because of their limitations in weight, power, and maintenance. In addition, as background noise and turbulence level increase with Mach number, the amplitude of excitation by the acoustic drivers would be insufficient to bring about a large change in the mean flow. Thus, any control by using low-amplitude excitation is not practical in many flows of engineering interest.[5]

Recently, various active control techniques using blowing/suction have been proposed for enhancing flow mixing. Raman[5] exploited

Received 5 April 2001; revision received 4 September 2001; accepted for publication 16 November 2001.

*Graduate Student, Department of Aerospace Engineering. Student Member AIAA.
†Graduate Student, Department of Aerospace Engineering; currently Design Engineer, Rolling Stock Design Section, Rolling Stock Technical Department, Nippon Sharyo, Ltd., 2-20 Honohara, Toyokawa, Aichi 442-8502, Japan.
‡Professor, Department of Aerospace Engineering. Member AIAA.

oscillating miniature fluidic jets to enhance mixing. Davis[6] used radial blowing from a pair of steady jets and obtained a variable control by adjusting the degree of penetration of the control jets into the main jet flow. Smith and Glezer[7] have been able to vector and mix jet flow by using synthetic jet or zero mass flow devices that require only electrical power and no fluid addition. A pulsed-jet version of this concept was developed and applied to the exhaust of a full-scale engine.[8] The pulsing jets induced the first azimuthal mode of the jet shear layer. The effect of enhanced mixing was seen in the substantially reduced temperature of the potential core along the engine centerline. Computational fluid dynamics (CFD) simulations of synthetic jets have been attempted by Cain et al.[9] using an unsteady Reynolds-averaged Navier–Stokes code and by Freund[10] using a direct numerical simulation code. These simulations verified the observed jet behaviors.[8] Nedungadi et al.[11] have investigated the higher antisymmetric modes of an array of synthetic jets and the effects on primary jet mixing and noise generation using CFD simulations.

In the present work, an experimental investigation of shear flow excitation using controllable unsteady microjets was conducted. The main motivation underlying this idea is to enhance jet mixing by exciting the jet shear flow using azimuthally distributed microjets. In the present study, the microjets were placed along the circumference of the nozzle exit of a primary jet at equal intervals and were directed toward the primary jet axis. Unsteady axisymmeric and antisymmetric, or flapping, actuation modes, as well as steady axisymmetric modes, are studied for both fully expanded and underexpanded primary jets.

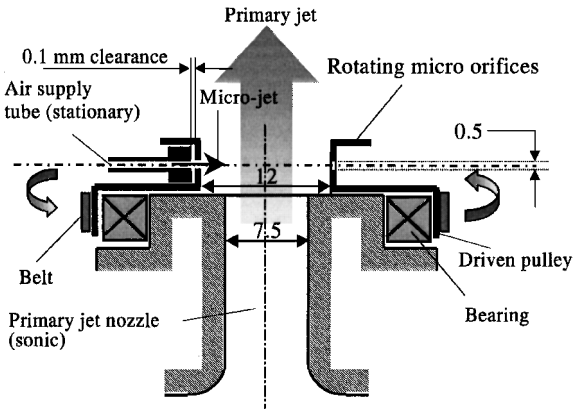

Fig. 1 Detailed schematic diagram of a single microjet relative to primary jet.

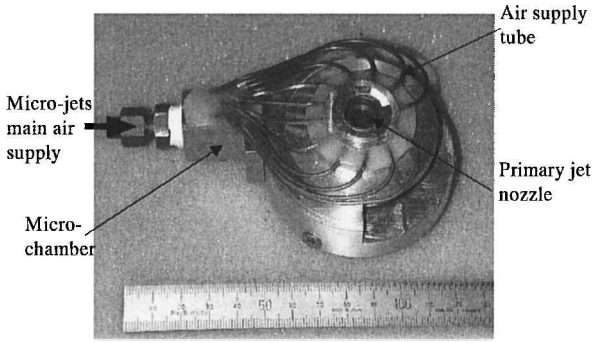

Fig. 2 Primary jet nozzle assembled with a microjet system.

II. Microjets Actuator

A. Axisymmetric Actuation

The arrangement of a single microjet is shown in Fig. 1. Figure 2 is a photograph of the actuator attached to the primary jet nozzle, where the system of 12 stationary pressure tubes is connected to the microchamber. The unsteady microjets actuator employed here consists of the following parts: 1) a circular microorifice plate supported by bearings, 2) stationary pressure tubes connected to a microchamber, and 3) a driving motor. The microorifice plate has 36 orifices, which are distributed along the circumference at 10-deg intervals. Each orifice has a diameter of 0.5 mm. The air supply tube system has 12 tubes that are placed at 30-deg intervals. These tubes are stationary, whereas the microorifice plate is allowed to rotate freely around the primary jet axis. A speed-controlled motor is employed to rotate the microorifices with a maximum rotational speed of 12,000 rpm. During the rotation, at the instant that the microorifices are aligned with the stationary air tubes, microjets are emitted toward the primary jet axis.

Figure 3a shows injection of microjets during one period τ in axisymmetric actuation mode. When the rotational frequency of the microorifices are changed, an arbitrary injection frequency can be realized according to the following formula:

$$f = 36 \times \Omega/60 \tag{1}$$

where f is the injection frequency in hertz and Ω is the rotational speed of motor, which is the same as that of the microorifices, in

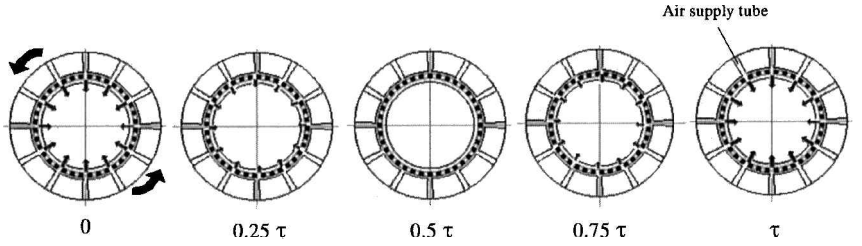

a) Axisymmetric actuation

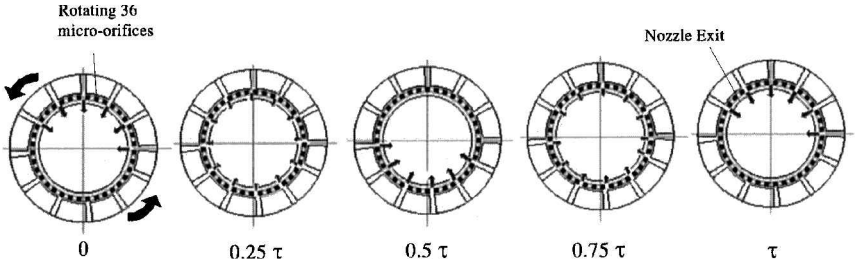

b) Antisymmetric, or flapping, actuation

Fig. 3 Cross-sectional view of microjets at primary jet nozzle exit during a complete injection cycle for both axisymmetric and antisymmetric modes.

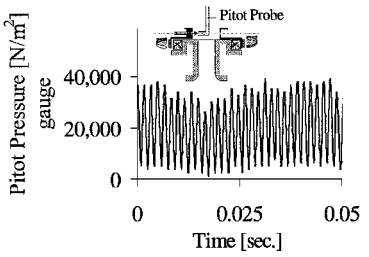

a) Time response of pressure

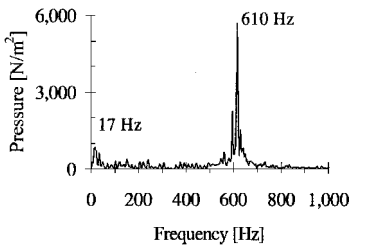

b) Spectrum

Fig. 4 Unsteady injection characteristics due to a single microjet with a microjet pressure ratio of 2.50 and a microorifice rotational speed of 1000 rpm.

revolutions per minute. Moreover, the amplitude of the unsteady microjet flow can be controlled by varying the microchamber pressure ratio P_μ/p_∞.

To examine the characteristics of the unsteady microjet flow, a pitot probe was placed facing the exit of the micronozzle at $P_\mu/p_\infty = 2.50$ and $\Omega = 1000$ rpm. Figure 4a shows the time response of the pitot probe. It is clearly seen that the signal shown in Fig. 4a has a high-frequency component that is superimposed on a low-frequency component. These two frequencies are also shown in the spectrum of a time signal in Fig. 4b. The high frequency is in agreement with that computed by Eq. (1), that is, the injection frequency of microjets, whereas the low frequency is close to the rotational frequency of the microorifices circular plate. This low frequency seems to be caused by the accuracy of fabrication. There may be slight differences in elevation between the microorifice holes, which could in turn appear as the time-varying signal of the rotational speed.

The injected mass fraction φ_j can be defined as the ratio of the injected mass to the mass flow rate of the primary jet flow. This ratio is a function of primary jet nozzle pressure ratio (NPR) and microjets pressure ratio NPR_μ. When φ_j and NPR are specified, the corresponding NPR_μ can be calculated by using the continuity equation for an isentropic flow. This computed NPR_μ will give the theoretical injected mass fraction. Although the actual injected mass fraction is considered to be less than the theoretical one, no attempt was made to measure the actual injected mass fraction. This loss in the injected mass fraction seems to occur because of a leakage due to a clearance between the microorifice plate and the air supply tubes, which is needed to reduce excessive friction at a high-speed rotation of microorifices.

B. Antisymmetric, or Flapping, Actuation

The antisymmetric mode was created by shifting the locations of six of the air supply tubes by 5 deg along the circumference. This would cause the two arrays of six microjets be emitted at two different instants, as shown in Fig. 3b.

Note that, although it was intended to excite only a single mode, in actual experiment several modes may be excited due to the finite number of microjets, the accuracy of actuator fabrication, and the transition process from closing and opening the microjets.

III. Experimental Setup

The experiment was conducted in the open jet facility at the Department of Aerospace Engineering, Nagoya University. A convergent (sonic) nozzle with an exit diameter of 7.5 mm was used to produce the primary jet flow. The nozzle is attached to a cylindrical plenum chamber that has a diameter of 220 mm and a length of 400 mm. For automatic flowfield measurements, a three-dimensional mechanical traverse with three stepping motors was employed. High-pressure air is supplied from a tank with a volume of 12 m^3 stored at a pressure of 12 kgf/cm^2 that is connected to the plenum chamber. A high-precision pressure regulator and a solenoid valve were used to control the pressure of the plenum chamber within a 0.25% accuracy.

The sound pressure level (SPL) was measured for acoustic properties by using a RION UC-29 1/4-in. (6.35-mm) condenser microphone that has a maximum frequency of 100 kHz and a maximum SPL of 160 dB. The microphone was traversed along an arc that is placed at a distance of $100D$ from the nozzle exit, where D is the diameter of the nozzle exit. The angle from the jet axis can be varied from 15 to 110 deg. The acoustic data were collected at a sampling rate of 100 kHz, and the spectrum of SPL was obtained by using a fast Fourier transform program.

The outside surfaces of the plenum chamber and other bodies placed in the near field were covered with two layers of acoustically absorbent, 6-mm-thick polyurethane foam to reduce strong reflections from the plenum chamber. Although the acoustic measurements were performed in a laboratory that was not acoustically lined, overall features of the emitted noise were well represented by the spectra, so that relative comparisons regarding the effect of jet actuation seem to be valid. In the present measurements, the background noise was 37.5 dB in a weighted SPL.

Most of the flowfield data were obtained by using a standard pitot probe with an outer diameter of 0.6 mm. This probe is connected to a KYOWA PA-5KB pressure transducer that has a maximum sampling frequency of 800 Hz and a limit pressure of 5 kgf/cm^2. A short dual-cone static pressure probe designed by Pinckney[12] at NASA Langley Research Center and used previously by Norum and Seiner[13] was employed for static pressure measurements in the case of underexpanded jet. The probe size was scaled down to fit it to the present nozzle geometry and to reduce the interference of the probe with the jet flow. The probe was calibrated inside a supersonic wind tunnel, and calibration results showed that the static pressure can be obtained with an error of 3%. This static probe is connected to a KYOWA PGM-2KC pressure transducer that has a maximum sampling frequency of 24,000 Hz and a limit pressure of 2 kgf/cm^2. Because the static pressure rises sharply downstream of a shock, the static probe can be used to examine the spacing and strength of the shock cell system. Despite errors caused by the probe intrusion, the measured shock cell spacings showed good agreement with those determined from schlieren pictures.

The Mach number distribution along the jet axis in the case of underexpanded jet was obtained by measuring both pitot and static pressures, where Rayleigh's supersonic pitot formula was applied to calculate the Mach number. On the other hand, in the case of fully expanded jet, the static pressure is constant and equal to the ambient pressure. Therefore, the centerline distribution of Mach number can be calculated directly from the pitot probe measurement alone by assuming an isentropic flow.

An ONO SOKKI HT-4100 digital tachometer, which can measure a maximum of 20,000 rpm, was employed to measure the rotational frequency of microorifices. Transducer zero errors were monitored before each run. The flow was also visualized for underexpanded jet by using a conventional two-mirror Töpler schlieren technique with a pulsed-light source of 10-μs duration.

IV. Results and Discussion

M_j is commonly used to denote the Mach number of a fully expanded jet and is uniquely related to the NPR, which is defined by P_t/p_∞ through the following equation:

$$M_j = \left\{\left[(P_t/p_\infty)^{\gamma-1/\gamma} - 1\right][2/(\gamma-1)]\right\}^{0.5} \tag{2}$$

The Mach number in the plume of an underexpanded supersonic jet can become actually higher than M_j. The pressure as well as the Mach number overshoots or undershoots the value in the fully expanded condition as the flow passes through the shock cell system. Note that M_j is nothing more than the exit Mach number of a fictitious nozzle, at whose exit the flow expands up to the given

Table 1 Experimental conditions

	Fully expanded jet 1			Fully expanded jet 2			Underexpanded jet		
Actuation mode	φ_j	NPR_μ	NPR	φ_j	NPR_μ	NPR	φ_j	NPR_μ	NPR
Baseline jet	0	1	1.89	0	1	1.89	0	1	3.00
Steady injection	0.04	1.5	1.89	0.06	2.15	1.89	0.04	2.25	3.00
Unsteady axisymmetric injection	0.04	1.5	1.89	0.06	2.15	1.89	0.04	2.25	3.00
Unsteady flapping injection case 1	0.04	2.80	1.89	0.06	4.3	1.89	0.04	4.50	3.00
Unsteady flapping injection case 2	0.02	1.50	1.89	0.03	2.15	1.89	0.02	2.25	3.00

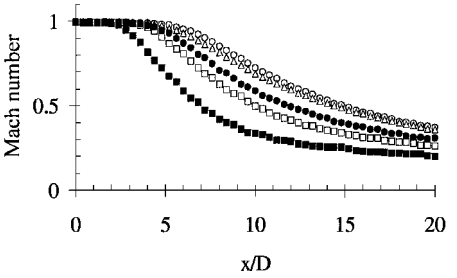

a) Centerline Mach number distribution

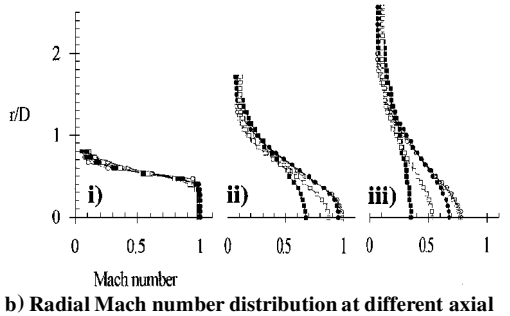

b) Radial Mach number distribution at different axial locations: i) $X/D = 1$, ii) $X/D = 5$, and iii) $X/D = 9$

Fig. 5 Fully expanded sonic jet: ○, baseline jet; △, axisymmetric steady mode; ●, unsteady axisymmetric mode; ■, unsteady flapping mode 1; and □, unsteady flapping mode 2; $Sr = 0.16$ and $\varphi_j = 0.04$ ($\varphi_j = 0.02$ for flapping mode 2).

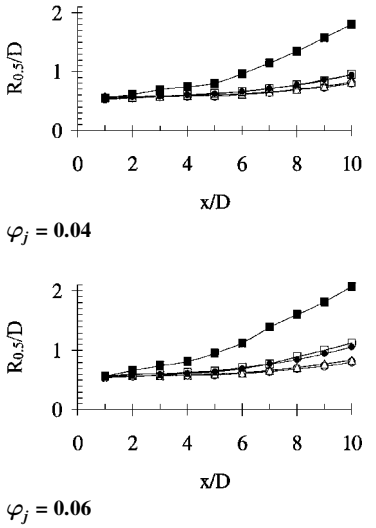

Fig. 6 Axial distribution of normalized jet radius $R_{0.5}/D$ for fully expanded jet with $M_j = 1$: ○, baseline jet; △, axisymmetric steady mode; ●, unsteady axisymmetric mode; ■, unsteady flapping mode 1; and □, unsteady flapping mode 2; $Sr = 0.16$.

NPR. In other words, it is an average jet Mach number in the region where the flow oscillates along the jet axis.

Two values of M_j were considered here: $M_j = 1.00$ for a fully expanded jet and $M_j = 1.36$ for an underexpanded jet, which correspond to NPR = 1.89 and 3.00, respectively. The corresponding Reynolds numbers are $Re = 1.5 \times 10^5$ and 1.4×10^5, respectively, which are based on the nozzle exit diameter and the primary jet velocity at the nozzle exit. Experimental conditions for the present study are listed in Table 1, which consists of two cases for a fully expanded jet and one case for an underexpanded jet. The unsteady microjets were injected at a frequency of 6300 Hz, which corresponds to a Strouhal number Sr of 0.16. This is close to one of subharmonics of the most amplified Strouhal number (see Ref. 14). As listed in Table 1, there are two flapping injections: In case 1 the theoretical injected mass flow rate is the same as those of both axisymmetric and steady injections, whereas in case 2, it is reduced by 50%. The second case was chosen because the mean flowfield was strongly affected in preliminary tests of the first case.

A. Mean Flowfields

1. *Fully Expanded Jet*

Figure 5a shows the centerline Mach number distribution of the fully expanded sonic jet for various injection modes at $Sr = 0.16$ and $\varphi_j = 0.04$, as well as that of the baseline jet. From Fig. 5, it is clearly seen that the centerline Mach in the cases of injection decays much faster than that of the baseline jet, which suggests an increase in jet spreading, or jet mixing.

The unsteady injections have higher spreading rates than the steady injection with case 1 of flapping injection, showing more dramatic change than case 2. The case of unsteady injection 2 is particularly interesting because even with a 50% reduction in the injected mass flow rate it produces a higher spreading rate than the axisymmetric modes. As will be detailed in Sec. IV.B, this is because antisymmetric disturbances are more unstable than axisymmetric ones, that is, the growth rate due to flapping actuation is higher than that due to the axisymmetric one. To see whether the flapping actuation bifurcates the jet, radial distributions of Mach number at several downstream locations were measured, the results of which are shown in Fig. 5b. As seen from Fig. 5b, it is confirmed that bifurcation does not take place in the present flows and that the Mach number distributions shown by Fig. 5a well represent the actual jet spreading.

Figure 6 shows the axial distribution of jet radius for two values of injected mass fraction, $\varphi_j = 0.04$ and 0.06. The jet radius is defined as the length from the axis to the location where the velocity becomes half the centerline velocity.[15] As shown in Fig. 6, the jet radius increases in the downstream direction, with case 1 of flapping mode having the higher rate.

2. *Underexpanded Jet*

To evaluate the actuator performance for a jet plume with a shock cell structure, the microjet actuation was applied to an underexpanded sonic jet with $M_j = 1.36$, which corresponds to NPR = 3.00. Figure 7 shows Mach number distributions of steady and unsteady axisymmetric modes and unsteady flapping modes, as well as the baseline jet, where $Sr = 0.16$ and $\varphi_j = 0.04$. The distributions were obtained by first measuring pitot and static pressures along the jet centerline and then applying Rayleigh's supersonic pitot formula. The results are characterized by wavy patterns of Mach number due to the standing shock/expansion structure inside the jet. The effect of microjet actuation on the distribution is qualitatively similar to that of the fully expanded jet with the same injected mass fraction. A reduction in the potential core length and shock strength due to the microjet actuation is clearly seen in Fig. 7. The potential core length is one of the most frequently used parameters to quantify

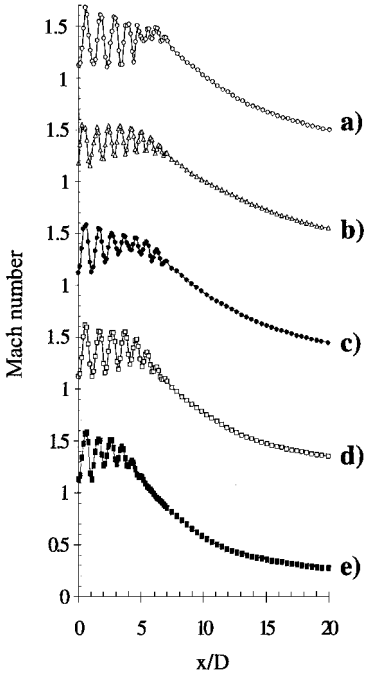

Fig. 7 Mach number distribution of underexpanded jet with $M_j = 1.36$: a) baseline jet, b) axisymmetric steady mode, c) axisymmetric mode, d) flapping mode 2, and e) flapping mode 1; $Sr = 0.16$ and $\varphi_j = 0.04$ ($\varphi_j = 0.02$ for flapping mode 2).

the mixing characteristics of a jet.[16] This length is defined as the distance measured in the axial direction from the nozzle exit to the location where the inside edge of the ring-shaped jet shear layer merges to a point at the axis. This length can be determined rather easily in the case of a fully expanded jet, where the centerline Mach number remains constant until the merging point and then decreases monotonically toward the downstream. In this study, the end of the potential core was defined as the location where the centerline Mach number drops to 5% below the nozzle exit Mach number.

The potential core length becomes harder to define in the case of the underexpanded jet because of the presence of a shock cell structure leading to significant oscillations in the centerline Mach number distribution. In an effort to overcome this difficulty, an average centerline Mach number was calculated by locally averaging the Mach number within each periodic shock cell. The potential core in the present study is then defined as the point where this locally averaged centerline Mach number begins to monotonically decrease below the averaged centerline Mach number measured in the upstream. Specifically, this averaged Mach number was obtained by averaging the Mach number distributions in the first four shock cells, which becomes close to that computed by Eq. (2).

Based on this definition, a reduction in the potential core length in the case of unsteady flapping mode 1 was 41 and 56% for underexpanded and fully expanded jets, respectively, for the same value of the injected mass fraction. Other actuation cases also showed similar trends of reduction in jet potential core length for both underexpanded and fully expanded jets, which are summarized in Fig. 8. Radial distributions of Mach number at several downstream locations are presented in Fig. 9, which confirm that jet bifurcation does not take place and that the Mach number distributions indicated in Fig. 7 represent the actual jet spreading. The underexpanded jet considered here was visualized by a schlieren method, the results of which (not shown here) confirm the measured mean flowfield shown in Fig. 7.

Figure 10 shows axial distributions of the jet radius. The two flapping modes have comparable effects on this parameter, which is different from the case of the fully expanded jet. As will be shown later, an increase in jet Mach number has a stabilizing effect on the fully expanded jets. As seen from the results of Fig. 10, the presence of a shock cell structure inside the jet plume has an opposite, destabilizing effect, especially for antisymmetric disturbances.

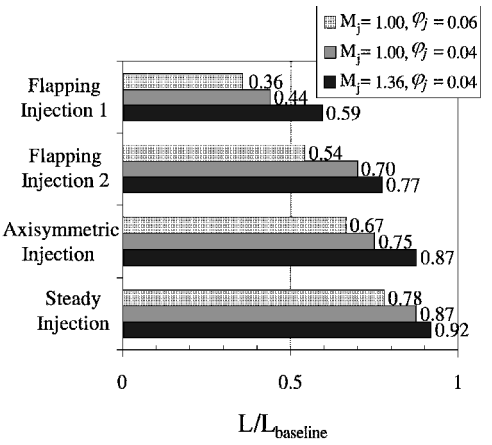

Fig. 8 Relative potential core length baseline jet for both fully expanded and underexpanded jets at $Sr = 0.16$ for unsteady injection.

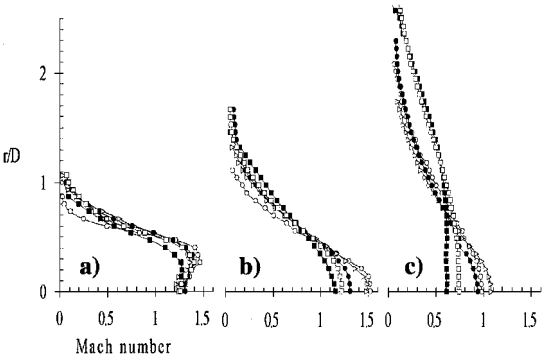

Fig. 9 Radial Mach number distribution at different axial locations: a) $x/D = 2$, b) $x/D = 5$, and c) $x/D = 10$ for underexpanded jet with $M_j = 1.36$: ○, baseline jet; △, axisymmetric steady mode; ●, unsteady axisymmetric mode; ■, unsteady flapping mode 1; and □, unsteady flapping mode 2; $Sr = 0.16$ and $\varphi_j = 0.04$ ($\varphi_j = 0.02$ for flapping mode 2).

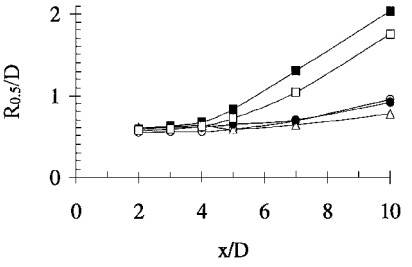

Fig. 10 Axial distribution of normalized jet radius $R_{0.5}/D$ for underexpanded jet with $M_j = 1.36$: ○, baseline jet; △, axisymmetric steady mode; ●, unsteady axisymmetric mode; ■, unsteady flapping mode 1; and □, unsteady flapping mode 2; $Sr = 0.16$ and $\varphi_j = 0.04$ ($\varphi_j = 0.02$ for flapping mode 2).

B. Linear Stability Analysis

Classical linear stability calculations are performed for the fully expanded jet considered in this study. In this analysis the main objectives are 1) qualitative understanding of how the disturbances grow downstream; 2) the effect of azimuthal disturbance mode, that is, the difference between axisymmetric and antisymmetric modes, on the stability; and 3) the role of compressibility in the stability. Only information essential to understand these results will be provided here. For details of the calculation procedure, the reader is referred to Michalke.[17]

The linear theory deals with small perturbations and linearized equations, so that it can only predict the initial, local growth of the small perturbations. However, some general insight into the development of large-scale structure in the jet can be obtained by examining the linear solution. A hyperbolic tangent velocity profile of the following form was used for the present calculation:

$$U(r)/U_0 = \tfrac{1}{2}\{1 + \tanh[0.25(R_{0.5}/\theta)(R_{0.5}/r - r/R_{0.5})]\} \quad (3)$$

Michalke,[17] Chan and Leong,[18] Morris,[19] Crigthon and Gaster,[20] and Plaschko[21] have also employed this profile for their jet stability analyses.

Note that $R_{0.5}/\theta$ in Eq. (3) is needed for the hyperbolic-tangent velocity profile at a given axial location. Therefore, the radial distributions of Mach number for the baseline jet, shown in Fig. 5b, along with the least-square fitting to the velocity profile of Eq. (3) are used to determine the axial variation of $R_{0.5}/\theta$ the results of which has the following form:

$$\theta/R_{0.5} = 0.060(X/D) + 0.015 \quad (4)$$

This relation is similar to the relations proposed by Crigthon and Gaster[20] and Plaschko[21] except for the constant value. This constant seems to depend on flow conditions at the nozzle exit.

It is convenient to relate the temperature to the velocity by the Busemann–Crocco law, which is valid for a boundary-layer flow with a constant pressure, as well as $Pr = 1$:

$$\frac{T(r)}{T_0} = \frac{T_\infty}{T_0} + \left(1 - \frac{T_\infty}{T_0}\right)\frac{U(r)}{U_0} + (\gamma - 1)M_0^2 \frac{U(r)}{U_0}\frac{[1 - U(r)/U_0]}{2} \quad (5)$$

where $T_\infty = T(\infty)$ is the ambient temperature.

In the present calculations, where spatially growing disturbances are considered, ω is taken to be real and n is an integer, whereas α is generally complex: $\alpha = \alpha_r + i\alpha_i$. The disturbances will be damped if $\alpha_i > 0$, neutral if $\alpha_i = 0$, and amplified if $\alpha_i < 0$.

Figure 11 presents the axial growth rate α_i, normalized by the momentum thickness vs the radian frequency ω, normalized by the momentum thickness and jet velocity, at three locations in the jet potential core region. The growth rates of disturbances for both zeroth (axisymmetric) mode with $n = 0$ and first (antisymmetric) mode with $n = 1$ are shown in Fig. 11. As we go downstream, the antisymmetric disturbances become more unstable than the axisymmetric ones. Note that this analysis is based on the local mean velocities of the baseline jet; therefore, the change in the mean velocity due to the growth of disturbances is neglected in the present analysis. Furthermore, this analysis assumes that the disturbances are small, which is not exactly applicable to the present case of microjet actuation. Therefore, the reason why the antisymmetric, or flapping, actuation is more effective than the axisymmetric one with regard to mixing can be deduced only qualitatively from the preceding results of stability analysis. In any case, it is clear from these results that the antisymmetric disturbances produced by the present antisymmetric actuation are more amplified in the downstream, which will change the mean flow more effectively than the axisymmetric actuation.

To see the effects of compressibility on jet stability, similar calculations were performed for the case of incompressible flow, that

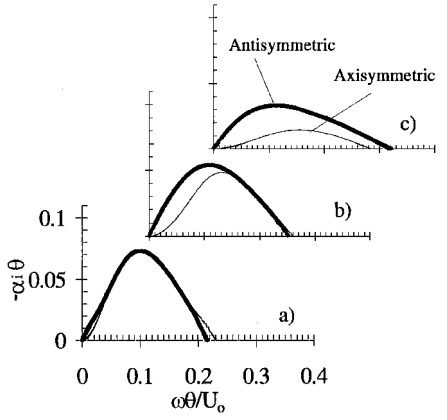

Fig. 11 Spatial growth rate $-\alpha_i$ vs frequency ω for both ——, axisymmetric and ——, antisymmetric disturbances at various axial locations in the region of jet potential core at $M_0 = 1$: a) $x/D = 0$, b) $x/D = 2$, and c) $x/D = 4$.

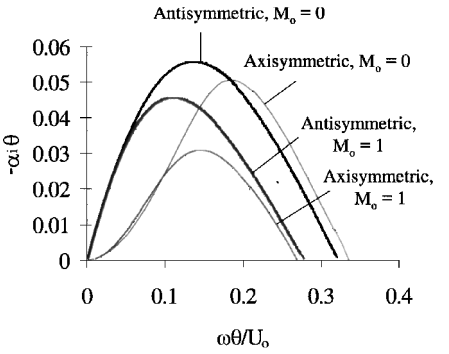

Fig. 12 Effects of compressibility on disturbance growth rate for velocity profile at $X/D = 3$.

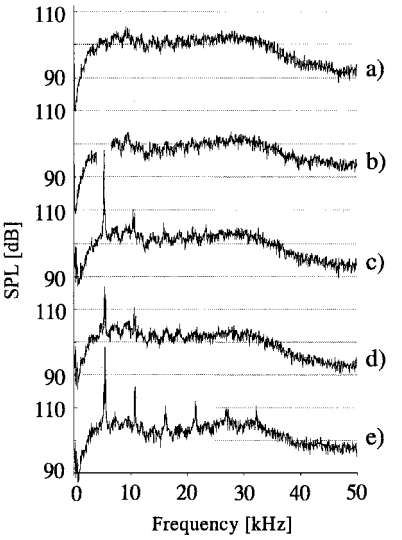

Fig. 13 Noise spectrum of fully expanded jet with $M_j = 1.00$: a) baseline jet, b) axisymmetric steady mode, c) axisymmetric unsteady mode, d) flapping mode 2, and e) flapping mode 1; $Sr = 0.16$ and $\varphi_j = 0.04$ ($\varphi_j = 0.02$ for flapping mode 2).

is, $M_0 = 0$, regarding both axisymmetric and antisymmetric modes, where the flow at $x/D = 3$ was employed as a base flow. The results are shown in Fig. 12, along with the compressible flow data at the same location of x/D. It turns out that the compressibility of jet flow has a stabilizing effect because the compressible flow is less unstable than the corresponding incompressible one. This will give an explanation for the effects of the actuation employed here on both the fully expanded and underexpanded jets, mentioned earlier.

Note that in this linear stability analysis the pressure field is held constant inside the jet plume. This is not the case for underexpanded jet with the shock cell structure. Consequently, the pressure is no longer constant inside the plume but overshoots or undershoots the ambient value. This pressure field seems to play an important role in destabilizing the jet flow, which can explain why the underexpanded jet with the case 2 of flapping mode, which has a reduced mass flow injection, has a comparable effect with the case 1, as shown in Fig. 10. This tendency was not seen in the cases of the fully expanded jet, as shown in Fig. 6, with regard to the axial distribution of jet radius. In short, the formation of shock cell structure has a strong destabilizing effect, especially for antisymmetric disturbances.

C. Jet Noise

The acoustic field responds strongly to the frequency of actuation and its harmonics when some external excitation is applied to a jet. Figures 13 and 14 show results of sound spectra for both fully expanded and underexpanded jets, respectively. A microphone is located in the acoustic field at an angle of 45 deg from the jet axis and $100D$ away from the nozzle exit. The underexpanded baseline jet is clearly characterized by a screech tone with a frequency of

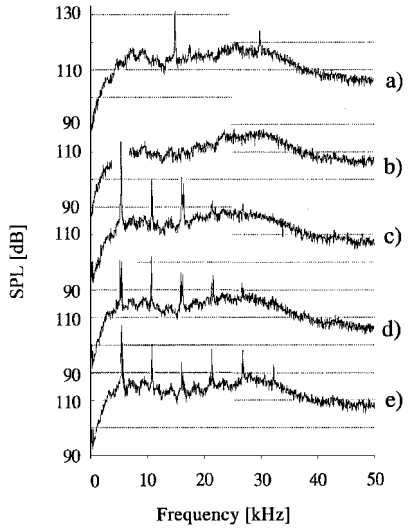

Fig. 14 Noise spectrum of underexpanded jet with M_j = 1.36: a) baseline jet, b) axisymmetric steady mode, c) axisymmetric unsteady mode, d) flapping mode 2, and e) flapping mode 1; Sr = 0.16 and φ_j = 0.04 (φ_j = 0.02 for flapping mode 2).

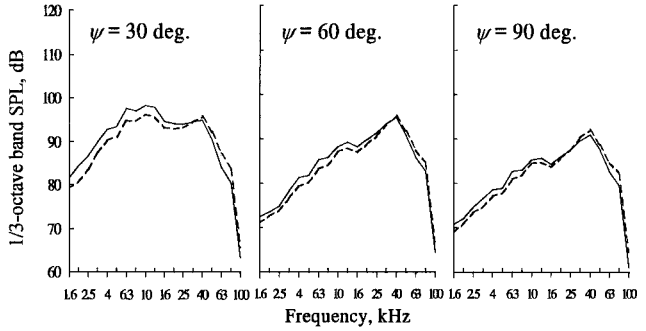

Fully expanded with M_j = 1.00

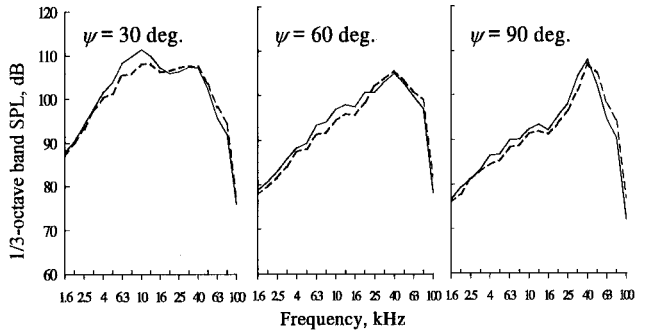

Underexpanded jet with M_j = 1.36

Fig. 15 One-third octave band SPL spectra at different emission angles: ——, baseline jet and – – –, axisymmetric steady injection; φ_j = 0.04.

15 kHz (Fig. 14a). Comparison of the results from the excited jets with those from the baseline jets indicates that natural and excited disturbances radiate noise in the downstream direction by a similar mechanism. Moreover, the results support the viewpoint that organized flow disturbances are directly responsible for a major portion of downstream noise radiation produced by the jet.[21] However, a reduction in the radiated noise was observed only in the steady injection cases for both fully expanded and underexpanded jets. This reduction seems to be due to mixing enhancement in a passive way such as in the case of vortex generators or tabs placed at the nozzle exit.[2]

Figure 15 shows the one-third octave band spectra in the axisymmetric steady injection cases shown in Figs. 13b and 14b, for both fully expanded and underexpanded jets at three different emission angles from the jet axis: 30, 60, and 90 deg. Results for the baseline

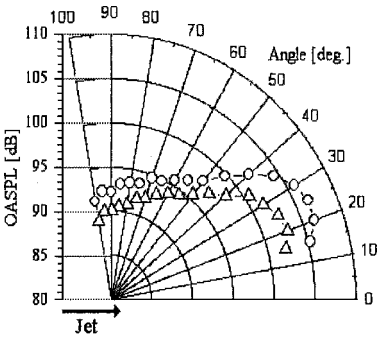

Fully expanded jet with M_j = 1.00

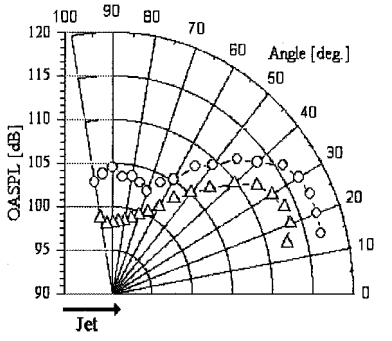

Underexpanded jet with M_j = 1.36

Fig. 16 OASPL directivity arc: ○, baseline jet and △, axisymmetric steady injection; φ_j = 0.04.

jets are also presented in Fig. 15 for comparison. The effect of actuation is clearly recognized as a reduction in SPL over most of the frequency range of the spectra, although the high-frequency portion is slightly increased. Mixing enhancement due to the steady actuation increases the high-frequency portion of the spectra. A similar effect due to tabs was reported in Ref. 2. The peak SPL at an emission angle of 30 deg is reduced by about 2–3 dB, whereas it does not change or slightly increases at the other two emission angles, 60 and 90 deg. Figure 16 shows directivity arcs for these cases, where a maximum reduction in the overall SPL (OASPL) is about 3–5 dB for both fully expanded and underexpanded jets.

V. Conclusions

Lateral steady or unsteady injection of an array of microjets placed along the circumference of the nozzle exit of a primary jet was experimentally studied to examine the characteristics of mixing and noise in compressible primary jets. Specifically, unsteady axisymmetric and flapping injection modes were employed in addition to steady axisymmetric injection. The unsteady injections were performed at an injection Strouhal number Sr of 0.16, based on the nozzle diameter and the primary jet velocity at the nozzle exit, which is close to one of the subharmonics of the most amplified Strouhal number obtained theoretically, for two cases of the total unsteady mass injection, 4 and 6% of primary jet mass flow rate.

The results of the mean flowfield showed that the flapping injection has a higher spreading rate than the steady or unsteady axisymmetric injection with regard to the decay of jet centerline velocity. Even when the unsteady mass injection is reduced by 50%, the antisymmetric mode grew and persisted farther downstream, that is, even in the flow downstream of the potential core region, compared with the case of axisymmetric mode with a full unsteady mass injection. These results were qualitatively confirmed by performing a linear stability analysis for the fully expanded jet, which showed that the antisymmetric mode of natural disturbances is more unstable than the axisymmetric one in the downstream region.

In the case of the underexpanded jet, the presence of the shock cell structure inside the jet plume has a strong destabilizing effect, especially for antisymmetric disturbances. This was confirmed by comparable effects of two different flapping actuations on the downstream evolution of the jet radius.

The radiated noise was reduced in the case of steady axisymmetric injection actuation, whereas it was increased in other cases of unsteady injection.

References

[1]Freund, J. B., and Moin, P., "Jet Mixing Enhancement by High-Amplitude Fluidic Actuation," *AIAA Journal*, Vol. 38, No. 10, 2000, pp. 1863–1870.

[2]Zaman, K. B. M. Q., Reeder, M. F., and Samimy, M., "Control of an Axisymmetric Jet Using Vortex Generator," *Physics of Fluids*, Vol. 6, No. 2, 1994, pp. 778–793.

[3]Longmire, E. K., Eton, J. K., and Elkins, C. J., "Control of Jet Structure by Crown-Shaped Nozzles," *AIAA Journal*, Vol. 30, No. 2, 1992, pp. 505–512.

[4]Zaman, K. B. M. Q., "Spreading Characteristics of Compressible Jets from Nozzle of Various Geometrics," *Journal of Fluid Mechanics*, Vol. 383, March 1999, pp. 197–228.

[5]Raman, G., "Using Controlled Unsteady Fluid Mass Addition to Enhance Jet Mixing," *AIAA Journal*, Vol. 35, No. 4, 1997, pp. 647–656.

[6]Davis, M. R., "Variable Control of Jet Decay," *AIAA Journal*, Vol. 20, No. 5, 1982, pp. 606–609.

[7]Smith, B., and Glezer, A., "Vectoring and Small-Scale Motions Effected in Free Shear Flows Using Synthetic Jet Actuators," AIAA Paper 97-0213, 1997.

[8]Kibens, V., Dorris, J., Smith, D. M., and Mossman, M. F., "Active Flow Control Technology Transition: The Boeing ACE Program," AIAA Paper 99-3507, 1999.

[9]Cain, A. B., Kral, L. D., Donovan, J. F., and Smith, T. D., "Numerical Simulation of Compressible Synthetic Jet Flows," AIAA Paper 98-0084, 1998.

[10]Freund, J. B., "Acoustic Sources in a Turbulent Jet: A Direct Numerical Simulaton Study," AIAA Paper 99-1858, 1999.

[11]Nedungadi, A., Barber, T. J., Nishmura, M., and Kudo, T., "The Effects of Pulsed Blowing on Jet Mixing and Noise Generation," AIAA Paper 2001-0665, 2001.

[12]Pinckney, S. Z., "A Short Static-Pressure Probe Design for Supersonic Flow," NASA TN-D 7978, 1975.

[13]Norum, T. D., and Seiner, J. M., "Measurement of Mean Static Pressure and Far-Field Acoustics of Shock Containing Supersonic Jets," NASA TM 84521, 1982.

[14]Raman, G., "Miniture Fluidic Oscillators for Flow and Noise Control," AIAA Paper 2000-2554, 2000.

[15]Troutt, T. R., and Mclaughin, D. K., "Experiments on the Flow and Acoustic Properties of a Moderate-Reynolds-Number Supersonic Jet," *Journal of Fluid Mechanics*, Vol. 116, March 1982, pp. 123–156.

[16]Shih, C., Alvi, F. S., and Washington, D. M., "Effects of Counterflow on the Aeroacoustic Properties of Supersonic Jet," *Journal of Aircraft*, Vol. 36, No. 2, 1999, pp. 451–457.

[17]Michalke, A., "Survey on Jet Instability Theory," *Progress in Aerospace Sciences*, Vol. 21, 1984, pp. 159–199.

[18]Chan, Y. Y., and Leong, R. K., "Discrete Acoustic Radiation Generated by Jet Instability," *Canadian Aeronautics and Space Institute Transactions*, Vol. 6, Sept. 1973, pp. 65–72.

[19]Morris, P. J., "The Spatial Viscous Instability of Axisymmetric Jets," *Journal of Fluid Mechanics*, Vol. 77, Oct. 1976, pp. 511–529.

[20]Crighton, D. G., and Gaster, M., "Stability of Slowly Diverging Jet Flow," *Journal of Fluid Mechanics*, Vol. 77, Sept. 1976, pp. 397–413.

[21]Plaschko, P., "Helical Instabilities of Slowly Diverging Jets," *Journal of Fluid Mechanics*, Vol. 92, May 1979, pp. 209–215.

P. J. Morris
Associate Editor